Correlation of Outer Retinal Degeneration and Choriocapillaris Loss in Stargardt Disease Using En Face Optical Coherence Tomography and Optical Coherence Tomography Angiography

TALAL ALABDULJALIL, RACHEL C. PATEL, ABDULLAH A. ALQAHTANI, SIMON S. GAO, MICHAEL J. GALE, MIAO ZHANG, YALI JIA, DAVID HUANG, PEI-WEN CHIANG, RUI CHEN, JUN WANG, RICHARD G. WELEBER, MARK E. PENNESI, AND PAUL YANG

• PURPOSE: This study measured and correlated degeneration of the junction between the inner and outer segments (IS/OS), the retinal pigment epithelium (RPE), and the choriocapillaris (CC) in Stargardt disease (STGD).

• DESIGN: Prospective cross-sectional study.

• METHODS: This study was conducted at the Casey Eye Institute. A total of 23 patients with STGD were enrolled and underwent optical coherence tomography angiography (OCTA). Scans were centered on the fovea. OCT slab projections and en face boundary maps were used to create masks to measure total IS/OS loss or RPE atrophy as well as regions of isolated IS/OS loss, isolated RPE atrophy, and matched IS/OS and RPE degeneration or intact IS/OS junction and RPE. CC vascular density (CCVD) was quantified from the CC angiogram. Outcomes included the area of loss, and the CCVD of degeneration in different areas was quantified and correlated.

• RESULTS: The total area of IS/OS loss was strongly correlated with the total area of RPE atrophy ($r = 0.96$; $P < 0.0001$) by a 1.6:1 ratio ($r^2 = 0.90$). CCVD within regions of matched degeneration (85.6% ± 2.7%; $P < 0.0001$), isolated IS/OS junction loss (93.6% ± 1.0%; $P = 0.0011$), and isolated RPE atrophy (94.1% ± 1.1%; $P = 0.0065$) were all significantly lower than normal (99.0% ± 0.17%). There was a trend for CCVD within intact areas (97.6% ± 0.38%) to decline as the area diminished ($r = 0.68$).

• CONCLUSIONS: Photoreceptor and RPE degeneration exhibited a strong relationship wherein the IS/OS loss was 1.6-fold greater than that of RPE atrophy, supporting the theory that photoreceptor degeneration precedes RPE in STGD. Both the photoreceptors and the RPE degeneration contributed synergistically to CCVD attenuation, but extralesional CCVD also tended to be abnormal. The findings and techniques in this study may be of utility in developing endpoints for clinical trials. (Am J Ophthalmol 2019;202:79–90. © 2019 Elsevier Inc. All rights reserved.)

ABCA4-RELATED RETINOPATHY, COMMONLY referred to as Stargardt disease (STGD) is an inherited macular dystrophy with a prevalence of 1 in 10,000 population and is typically associated with mutations in the *ABCA4* gene, which are inherited in an autosomal recessive manner.[1] Although STGD commonly presents as a maculopathy characterized by yellow pisciform-shaped fleck deposits and macular atrophy,[2] there are more severe phenotypes that present with generalized cone or cone-rod dysfunction.[3–5] Additionally, less severe phenotypes, previously referred to as fundus flavimaculatus, can manifest with pisciform deposits extending to the mid-periphery but without central atrophy.[6,7] The STGD spectrum has also been categorized based on age of onset, wherein the early onset group of 10 years or younger exhibits more severe disease and rapid decline in visual acuity,[8] whereas the late-onset group of 45 years of age or older typically has milder disease with preserved fovea and visual acuity for many years.[5,7,9–11] The severity of STGD has also been classified by the level of retinal dysfunction as measured by the full field electroretinogram (ERG).[12,13] Rarely, mutations in the *ABCA4* gene have also been implicated in retinitis pigmentosa.[14,15]

Mutations in the *ABCA4* gene result in a loss of function in the encoded flippase protein that leads to progressive accumulation of all-trans-retinal and *N*-retinylidene-phosphatidylethanolamine, which irreversibly forms di-retinoid-phosphatidylethanolamine (A2PE) in the

AJO.com Supplemental Material available at AJO.com.

Accepted for publication Feb 6, 2019.

From the Casey Eye Institute (T.A., A.A.A., S.S.G., M.J.G., Y.J., D.H., P.-W.C., R.G.W., M.E.P., P.Y.), Oregon Health and Science University, Portland, Oregon, USA; Albahar Eye Center, Ibn Sina Hospital, Ministry of Health, Kuwait (T.A.); Department of Ophthalmology, College of Medicine, Imam Abdulrahman Bin Faisal University, Dammam, Saudi Arabia (A.A.A.); Genentech, South San Francisco, California, USA (S.S.G.); Topcon Healthcare Solutions, Milpitas, California, USA (M.Z.); and Department of Molecular and Human Genetics, Baylor College of Medicine, Houston, Texas, USA (R.C., J.W.).

Inquiries to Paul Yang, 3375 SW Terwilliger Boulevard, Portland, OR 97239, USA; e-mail: yangp@ohsu.edu

0002-9394/$36.00
https://doi.org/10.1016/j.ajo.2019.02.007

photoreceptor outer segments and, in turn, leads to accumulation of di-retinoid-pyridinium-ethanolamine (A2E) in the retinal pigment epithelium (RPE).[16–25] It is believed that the aforementioned bisretinoids and their precursors may be photooxidized to generate cytotoxic compounds, but it remains to be determined which ones directly cause photoreceptor versus RPE cell death.[16] Moreover, the accumulation and photooxidation of bisretinoids are interrelated to the activation of a complement system and accumulation of membrane attack complex, which exacerbate cell death in STGD.[26–29] To further elucidate the pathophysiology of STGD, highly detailed volumetric in vivo imaging of the photoreceptor and RPE layers in patients with STGD is now possible with recent advancements in optical coherence tomography (OCT) technology.

With the advent of ultra-high speed OCT, detailed en face structural data can be extracted from the volumetric OCT data and quantified using semi-automated segmentation software.[30,31] Moreover, through the detection of motion and flow over time, OCT angiography (OCTA) provides novel information about retinal and choroidal vasculature, which has the following advantages over conventional dye-based angiography: 1) it is a non-invasive procedure in that intravenous dye is not required; 2) it allows registration and tracking for comparative follow-up studies; and 3), it produces 3-dimensional (3D) flow information of retinal vessels and choriocapillaris (CC) that is quantifiable and not confounded by dye extravasation.[32,33] In this study, we use en face OCT and OCTA to characterize the dynamics of structural and vascular degeneration, respectively, of the retina and CC in patients with STGD.

METHODS

THIS WAS A PROSPECTIVE CROSS-SECTIONAL STUDY OF 23 patients (46 eyes) who had a clinical diagnosis of STGD, recruited between July 2015 and June 2016 from the Ophthalmic Genetics Clinic at Casey Eye Institute. The study protocol was approved prospectively by Oregon Health and Sciences University institutional review board, following the tenets of the Declaration of Helsinki, and complied with the Health Insurance Portability and Accountability Act. The institutional review board approved the collection and analysis of de-identified clinical history, ocular imaging, and genetic test results. Informed consent was obtained from all participants. Inclusion criteria were a diagnosis of autosomal recessive STGD based on the pedigree and clinical phenotype of fleck deposits with or without genetic testing or at least 2 pathogenic mutations in the *ABCA4* gene. The exclusion criteria were history of concurrent retinal disease of another cause or the presence of motion or media-opacity artifact in the OCTA image.

All patients received an ophthalmic examination including fundus autofluorescence (AF) using either the Optos (200Tx confocal scanning laser ophthalmoscope; Optos PLC, Marlborough, Massachusetts) or Spectralis (Heidelberg Engineering, Heidelberg, Germany) imaging systems and OCTA imaging (RTVue-XR Avanti with AngioVue; OptoVue Inc., Fremont, California). The OCTA scans contained both volumetric flow (decorrelation) data and volumetric structural (reflectance) data, which covered 6×6 mm^2 and were centered over the fovea (Figure 1). Our custom-made reading software, COOL-ART (Center for Ophthalmic Optics and Lasers-Angiography Reading Toolkit)[34] was used to segment retinal layers and generate en face thickness maps. The slabs used to create en face OCT images of the inner segment/outer segment (IS/OS) junction and RPE were each 9 μm thick, and the position of the slabs was manually optimized for each eye (Figure 1a and b). Using custom-made Matlab software (Natick, Massachusetts), a panel of experts (T.A., A.A.A., R.C.P., and S.S.G.) determined the exact position of the OCT slabs to best capture information for degeneration of the IS/OS junction and the RPE layers. The IS/OS slab was positioned to include the hyperreflective IS/OS band on OCT B-scans. To detect RPE atrophy and avoid Bruch's membrane, the RPE slab encompassed only the apical one-third of the hyperreflective RPE band on OCT B-scans with manual adjustment of ± 1 to 2 pixels as needed. Even though en face OCT and AF imaging of RPE atrophy are correlated to loss of melanin versus lipofuscin, respectively, prior studies have shown that there is good agreement for the detection of RPE atrophy between the 2 modalities in STGD.[35] Therefore, corresponding AF images were used for reference to ensure there were no gross errors with the final slab position.

Once the 6×6 mm^2 en face slab projections of the IS/OS and RPE layer were created, 3 experienced graders (T.A., A.A.A., and M.J.G.) used the freehand selection tool in ImageJ version 2.0 (open source, National Institutes of Health, Bethesda, Maryland) to outline the areas of IS/OS layer loss and RPE layer (Figure 1c and d). Graders were instructed to continuously review the B-scans during the grading process to ensure the masking accurately reflected the anatomical loss. Graders were blinded to each other's results. No normal results were used for controls, given that healthy macula have no RPE or IS/OS loss so there is nothing to grade. The outlined boundaries of degeneration were used as maps to create an IS/OS loss mask or RPE atrophy mask, wherein areas of degeneration could be quantified (Figure 1e). Among the three graders, areas of IS/OS loss or RPE atrophy were analyzed for correlation statistics and subsequently averaged for further statistical analysis.

Representative boundary masks from 1 grader (T.A.) were used for additional analysis. Using the "Subtract" and "And" functions from the ImageJ calculator tool, the

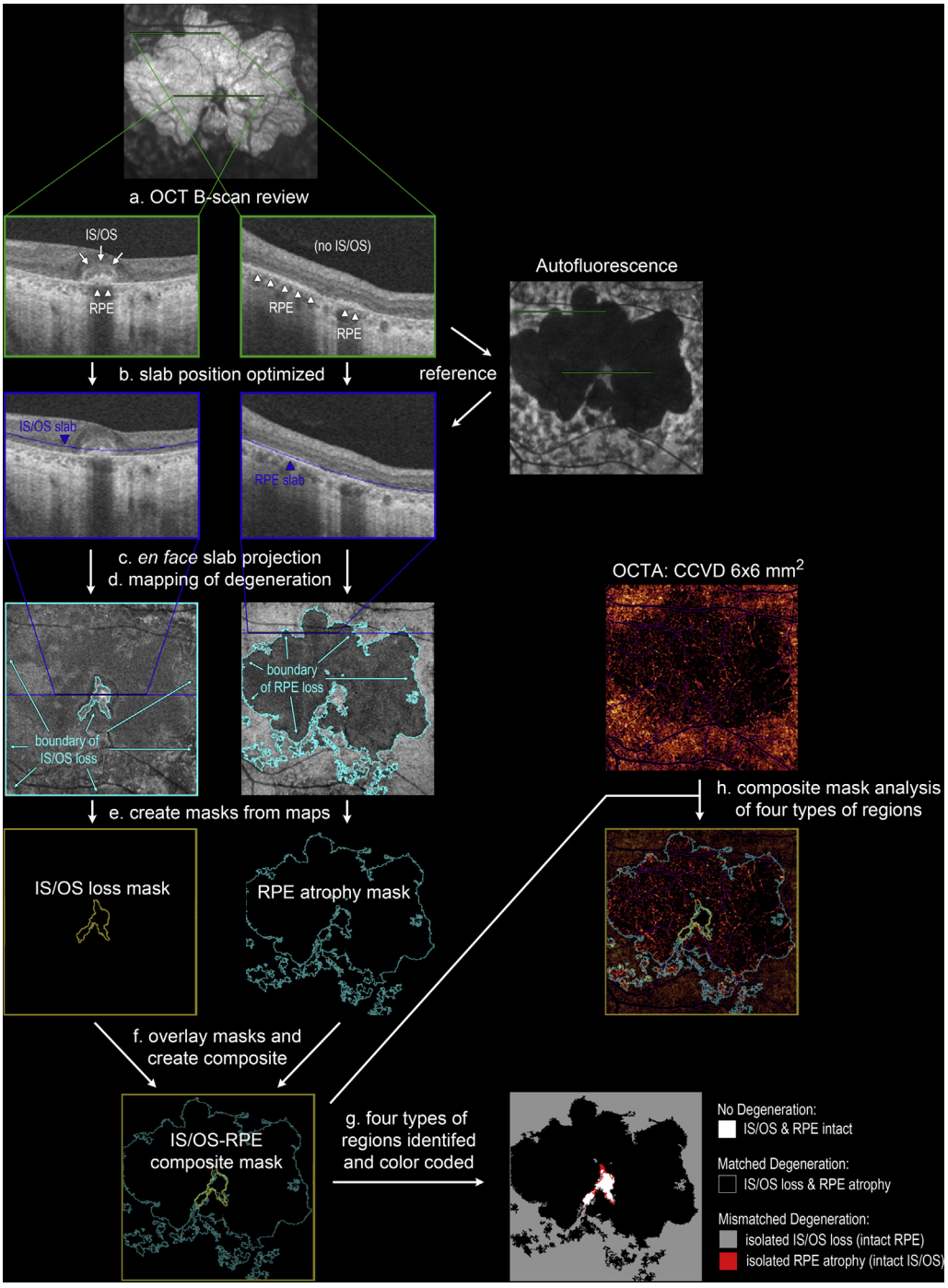

FIGURE 1. Methods for en face slab projection, boundary maps, and mask analysis. Sample images from patient 2 show 1 B-scan with preserved IS/OS junction and RPE and another with only isolated RPE atrophy (a). Slab position (blue line) is optimized manually for both IS/OS and RPE layers using autofluorescence images as references for the later (b). The en face projections of the IS/OS junction and the RPE slab are shown along with the boundary lines (cyan) of IS/OS and RPE atrophy, respectively, from 1 grader (c and d). The IS/OS loss mask (dark yellow) and RPE atrophy mask (dark cyan) are created from the boundary maps (e) and then overlaid to create the IS/OS-RPE composite mask (f). The composite mask identifies 4 types of regions of degeneration, which are used for the analysis of area (g) and CCVD (h). CCVD = choriocapillaris vascular density; IS/OS = inner section/outer section; OCTA = optical coherence tomography; RPE = retinal pigment epithelium.

TABLE 1. Patient Demographics and Genotype

Patient	Sex	Age (y)	*ABCA4* allele 1	*ABCA4* allele 1
1	F	14	c.5882G>A	c.4469G>A
2	F	62	c.1222C>T	ND
3	M	35	TD	TD
4	M	35	c.5714+5G>A	c.2894A>G
5	F	19	c.6449G>A	c.5196+1137G>A
6	F	25	c.4537C>G	ND
7	M	21	c.5882G>A	c.4139C>T
8	F	59	c.2041C>T	ND
9	M	55	c.5196+1137G>A	c.4774-27T>C
10	F	19	c.2588G>C	c.1222C>T
11	M	53	c.5461-10T>C	ND
12	F	56	c.2947A>G	ND
13	F	21	c.1622T>C	c.3113C>T
14	F	42	c.4222T>C	c.4918C>T
15	F	13	c.4739T>C	c.4469G>A
16	F	52	TD	TD
17	M	26	c.4457C>T	c.5461-10T>C
18	F	55	TD	TD
19	F	16	c.5714+5G>A	c.4469G>A
20	M	56	c.4234C>T	ND
21	F	49	c.6229C>T	890 bp deletion[a]
22	F	48	c.5899-2delA	ND
23	F	23	c.2588G>C	c.161G>A
	Male = 7	Mean = 37	2 alleles identified (n = 13)	
	Female = 16	SD= 17.1	1 allele identified (n = 7)	
			TD n= 3	

bp = base pair; F/M = female/male; ND = not detected; TD = testing declined.
[a]Spanning exons 28 and 29.

IS/OS loss maps and RPE atrophy maps for each eye were overlaid to create a composite map (Figure 1f) that defined 4 types of regions in each eye: 1) common areas of matching IS/OS loss and RPE atrophy; 2) common areas of matching IS/OS and RPE preservation, as well as areas of mismatched degeneration wherein 3) IS/OS was lost in isolation with intact RPE; or 4) RPE was atrophic in isolation with intact IS/OS (Figure 1g). The boundary maps of these 4 regions were used as masks to quantify the area of each respective region for each eye.

A commercial version of a split-spectrum amplitude decorrelation angiography algorithm was used in the AngioVue system[36] to compute flow signal and generate volumetric OCTA scans (304 × 304 × 640 pixels).[37] We used the COOL-ART[34] software to semi-automatically detect the outer boundary of Bruch's membrane, and the CC angiogram (6 × 6 mm^2) was generated by projecting the angiographic signal from 9 to 15 μm below the outer boundary of Bruch's membrane. Shadow graphic projection artifacts from large retinal blood vessels were minimized by a previously described technique.[33] CC vascular density (CCVD), which is defined as the percentage of area occupied by CC blood vessels, was evaluated for the entire en face angiogram in both STGD patients and normal subjects.[38] The CCVD was also calculated for the areas defined by the boundary masks, as described above for STGD patients (Figure 1h). Separate graders who were blinded to the masking analysis analyzed the images for CCVD in STGD patients and in normal subjects.

All data from the right and left eyes of each patient were highly correlated (data not shown), and thus the averaged values of both eyes were used to represent each patient. Non-parametric linear regression analysis, non-parametric analysis of variance (ANOVA) (Kruskal-Wallis), Mann-Whitney *U*, and Spearman correlation were used for statistical analysis. The Dunn-Bonferroni correction were used for multiple comparisons. To determine intergrader agreement, intraclass correlation coefficients with 95% confidence intervals (CI) were calculated.

RESULTS

IN OUR COHORT OF 23 PATIENTS WITH STGD, THE MEAN AGE was 37 years old (range: 13–62 years of age) with a

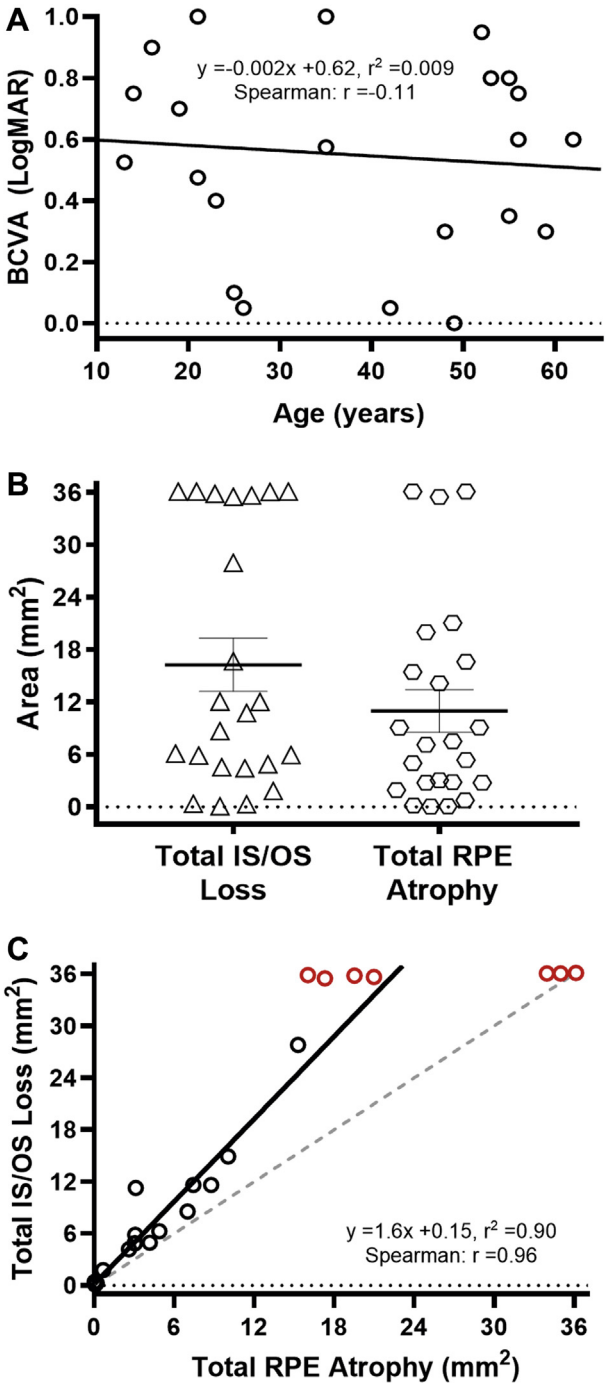

FIGURE 2. Age versus BCVA and total RPE atrophy versus total IS/OS junction loss. (A) Scatter plot of age versus BCVA, which shows no correlation. (B) On average, total IS/OS loss tended to be greater than total RPE atrophy; however it was not statistically significant, and the data was skewed by the floor effect of complete loss of layers (36 mm^2) in 6 patients for IS/OS loss and 3 patients for RPE atrophy. (C) Scatter plot of total RPE atrophy versus IS/OS atrophy shows a strong correlation, excluding data points that suffer from the floor effect (red circles). For reference, the dotted line represents a 1:1 relationship. BCVA = best-corrected visual acuity; IS/OS = inner segment/outer segment; RPE = retinal pigment epithelium.

preponderance of females at approximately a 2:1 ratio. Thirteen patients (57%) possessed two *ABCA4* pathogenic mutations, 7 patients (30%) had only 1 identified pathogenic mutation, and 3 patients declined genetic testing (Table 1). The mean best-corrected visual acuity (BCVA) at the time of imaging was 20/70 (range: 20/20–20/200) or 0.55 ± 0.31 LogMAR (range: 0.0–1.0 LogMAR). Correlation analysis did not show that age was significantly correlated with BCVA, which is not surprising given this is not a longitudinal study but rather a cross-sectional study of a heterogeneous population of STGD patients with early or late onset disease with or without foveal atrophy (Figure 2A).

The areas of degeneration calculated using masks from the boundary maps of total IS/OS loss or RPE atrophy among the 3 graders were highly correlated with intraclass correlation coefficients of and 0.998 (95% CI: 0.997–0.999) and 0.985 (95% CI: 0.971–0.993), respectively. Among STGD patients, there was a large spectrum of total IS/OS loss (range: 0.090–36 mm^2) and RPE atrophy (range: 0.037–36 mm^2), with a trend toward the average area of degeneration for IS/OS greater than that for RPE (16.10 ± 3.04 mm^2 vs 10.97 ± 2.39 mm^2, respectively; $P = 0.20$) (Figure 2B). Indeed, within the imaged area, 7 patients had complete loss (~36 mm^2) of IS/OS, of whom 3 also had complete loss of RPE. In other words, no patient had complete loss of RPE without also having complete loss of IS/OS. Excluding the floor effect of data points with complete loss (Figure 2, red circles), the total IS/OS loss and total RPE atrophy were strongly correlated with each other ($r = 0.96$, $P < 0.0001$), and linear regression showed the data were best fitted by a linear equation with a slope of 1.6 ($r^2 = 0.90$) (Figure 2C). These data describe a relationship in which IS/OS loss is 1.6 times more widespread than RPE atrophy in STGD. Total IS/OS loss and RPE atrophy were only moderately correlated with age ($r = 0.48$ and 0.49, respectively) or BCVA ($r = 0.61$ and 0.49, respectively) but were not significant after correction for multiple comparisons (Table 2, Figure S1).

Composite IS/OS-RPE masks were created from IS/OS loss and RPE atrophy masks, with the exception of data with a floor effect of complete IS/OS and RPE degeneration within the 6 × 6 mm^2 area of analysis, which were excluded. The composite masks revealed 4 types of regions, which were color coded in Figure 3 as follows: black represents areas of matching degeneration of IS/OS loss and RPE atrophy, white represents matching areas of intact IS/OS and RPE, gray represents areas of mismatched degeneration with intact RPE and isolated IS/OS loss, and red represents areas of mismatched degeneration with intact IS/OS and isolated RPE atrophy (Figure 3A). There were similar amounts of matching degeneration for IS/OS loss and RPE atrophy (47%, 3.87 ± 0.93 mm^2), as there were for mismatched degeneration of either isolated IS/OS loss or isolated RPE atrophy (53%, 4.41 ± 1.07 mm^2) (Figure 3B). Among the areas of mismatched degeneration,

TABLE 2. Correlation Statistics[a]

Age compared with	Spearman *r*	*P* value	BCVA compared with	Spearman *r*	*P* value
BCVA	−0.1127	0.6085	-	-	-
Total IS/OS loss	0.4833	0.0195	Total IS/OS loss	0.6053	0.0022
Total RPE atrophy	0.4853	0.0189	Total RPE atrophy	0.5929	0.0029
Isolated IS/OS loss	0.5312	0.0132	Isolated IS/OS loss	0.2245	0.3280
Isolated RPE atrophy	0.2446	0.2852	Isolated RPE atrophy	−0.3626	0.1062
Matched loss	0.5892	0.0049	Matched loss	0.4945	0.0227
Mismatched loss	0.5260	0.0143	Mismatched loss	0.2375	0.3000
CCVD (6 × 6 mm^2)	−0.5036	0.0143	CCVD (6 × 6 mm^2)	−0.4736	0.0224
Total IS/OS loss compared with			Total RPE atrophy compared with		
Total RPE atrophy[a]	**0.9647**	**< 0.0001**	-	-	-
Isolated IS/OS loss[a]	**0.9265**	**< 0.0001**	**Isolated IS/OS loss[a]**	**0.8331**	**< 0.0001**
Isolated RPE atrophy	0.5077	0.0466	Isolated RPE atrophy	−0.0301	0.8998
Matched loss[a]	**0.8643**	**< 0.0001**	**Matched loss[a]**	**0.9910**	**< 0.0001**
Mismatched loss[a]	**0.9324**	**< 0.0001**	**Mismatched loss[a]**	**0.8406**	**< 0.0001**
CCVD (6 × 6 mm^2)[a]	**−0.7684**	**< 0.0001**	**CCVD (6 × 6 mm^2)[a]**	**−0.7459**	**0.0002**
Isolated IS/OS loss compared with			Isolated RPE atrophy compared with		
Isolated RPE atrophy	−0.1677	0.4797	-	-	-
Matched loss[a]	**0.8389**	**< 0.0001**	Matched loss	−0.0663	0.7813
Mismatched loss[a]	**0.9744**	**< 0.0001**	Mismatched loss	−0.0745	0.7550
CCVD (6 × 6 mm^2)[a]	**−0.6917**	**0.0007**	CCVD (6 × 6 mm^2)	0.2505	0.2868
CCVD (isolated IS/OS loss)	−0.1233	0.6045	CCVD (isolated RPE atrophy)	0.2420	0.4015
Matched loss vs.			Mismatched loss compared with		
Mismatched loss[a]	**0.8313**	**< 0.0001**	-	-	-
CCVD (6 × 6 mm^2)[a]	**−0.7620**	**< 0.0001**	CCVD (6 × 6 mm^2)	−0.4948	0.0226
CCVD (matched loss)	−0.4834	0.0308	Intact IS/OS+RPE compared with		
			CCVD (intact IS/OS+RPE)	0.6842	0.0017

BCVA = best-corrected visual acuity; CCVD = choriocapillaris vessel density; IS/OS = inner segment/outer segment junction; Matched loss = total area of both IS/OS loss and RPE atrophy; Mismatched loss = total area of either isolated IS/OS or RPE atrophy; RPE = retinal pigment epithelium.

[a]Values and designations in boldface indicate comparisons that remain significant after Bonferonni correction for multiple comparisons ($P \leq 0.0013$ for significance).

there was significantly greater areas of isolated IS/OS loss (86%, 3.79 ± 1.0 mm^2) than isolated RPE atrophy (14%, 0.63 ± 0.15 mm^2; $P = 0.0005$) (Figure 3C), which indicates that photoreceptor IS/OS degeneration is more widespread than RPE atrophy and commonly spreads into areas of intact RPE in STGD. The area of total IS/OS loss or total RPE atrophy was strongly and significantly correlated with matched degeneration ($r = 0.86$ or 0.99), mismatched degeneration ($r = 0.93$ or 0.84), and isolated IS/OS loss ($r = 0.93$ or 0.83) but not isolated RPE atrophy ($r = 0.51$ or −0.03; Table 2; Figure S2). Moreover, the area of isolated IS/OS loss was strongly and significantly correlated with matched or mismatched degeneration ($r = 0.84$ or 0.97), but isolated RPE atrophy was not ($r = -0.066$ or −0.075) (Table 2, Figure 4). These data indicate that, as the overall area of degeneration enlarges, the various types of regions identified by composite masking also enlarge proportionately, except for isolated RPE atrophy, which was uncommonly observed and tended to be associated with rare IS/OS tubulations.

Analysis of the CC by OCTA within the total 6 × 6 mm^2 area showed that there was a trend toward declining CCVD with increasing age in STGD patients but that the correlation was moderate ($P = -0.50$) and lost significance when corrected for multiple comparisons, whereas normal subjects had relatively stable CCVD over time (Table 2, Figure 5A). The normal individuals had a mean age of 34 (range: 24–49 years of age; n = 10). There was also a moderate correlation between declining CCVD and worsening BCVA ($r = -0.47$), but that correlation also lost significance after Bonferroni correction (Table 2, Figure 5B). The total CCVD in STGD patients (92.0 ± 2.0%) was significantly lower than in normal subjects (99.0 ± 0.17%; $P = 0.0044$) (Figure 5C) and was negatively correlated with greater areas of total IS/OS loss ($r = -0.77$), total RPE loss ($r = -0.75$), matched degeneration ($r = -0.76$), and isolated IS/OS loss ($r = -0.69$) but not with isolated RPE atrophy (Figure S3). These results showed that total CCVD attenuation had a much stronger relationship with the severity of photoreceptor and RPE

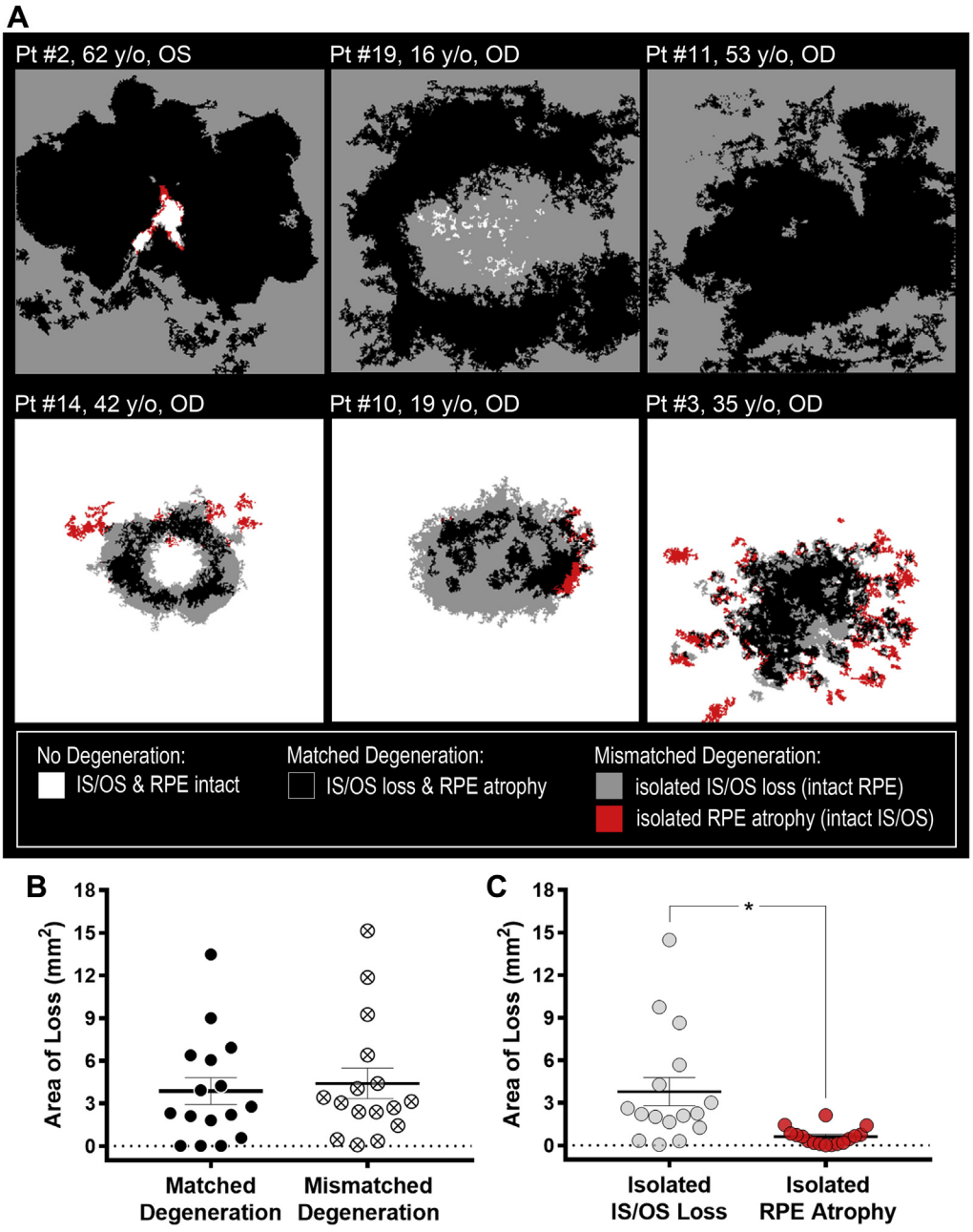

FIGURE 3. Composite mask analysis in the area of loss. (A) Sample images of composite analysis, which is color-coded to show the 4 different patterns of degeneration: areas of no degeneration (white), areas of matched degeneration (black), areas of isolated IS/OS junction loss (gray), and areas of isolated RPE atrophy (red). Patients 2, 19, and 11 show large areas of matched degeneration and isolated IS/OS loss, whereas patients 3, 10, and 14 show diffusely intact IS/OS and RPE with central areas of mixed types of degeneration. Both patient 2 and 14 show foveal preservation of IS/OS and RPE. Overall, isolated RPE atrophy was not common. (B) On average, the area of matched degeneration was similar to the area of mismatched degeneration (isolated IS/OS loss + isolated RPE atrophy). (C) The area of isolated IS/OS loss was significantly greater than the area of isolated RPE atrophy. *P = 0.0005. IS/OS = inner segment/outer segmen; RPE = retinal pigment epithelium.

degeneration than with age or BCVA. Moreover, isolated RPE atrophy was uncommon and likely contributed too small an area to have a significant relationship with total CCVD.

Composite IS/OS-RPE masks were also used to analyze the CCVD within the 4 types of regions. Regions with areas near zero were excluded from analysis because CCVD could not be meaningfully assessed. The CCVD within regions of

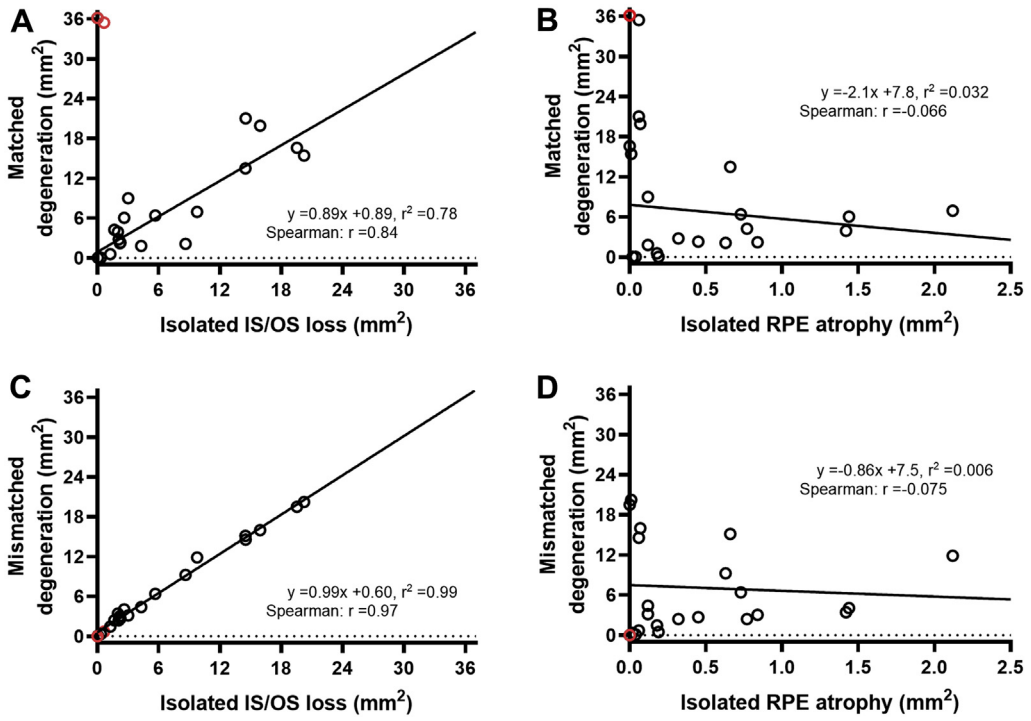

FIGURE 4. Correlation analysis of region types of degeneration. (A and B) Scatter plots of isolated IS/OS loss versus matched or mismatched degeneration show a strong correlation. (C and D) Scatter plots of isolated RPE atrophy versus matched or mismatched degeneration show no correlation. Data points with floor effect (red) were excluded from analysis. IS/OS = inner segment/outer segment; RPE = retinal pigment epithelium.

matched degeneration (85.6 ± 2.7%), isolated IS/OS loss (93.6 ± 1.0%), and isolated RPE atrophy (94.1 ± 1.1%) were all significantly lower than the CCVD loss in normal subjects (99.0 ± 0.17%; $P < 0.0001$, $P = 0.0011$, and $P = 0.0065$, respectively) (Figure 5C). However, there were no significant differences among the CCVD within regions of isolated IS/OS loss, isolated RPE atrophy, or matched degeneration ($P > 0.99$). These data show that either IS/OS or RPE degeneration may independently contribute to a similar decline in CCVD, which tended to be milder than that associated with combined IS/OS and RPE attenuation.

There was no correlation between the CCVD within regions of isolated IS/OS loss or isolated RPE atrophy and the size of the area of degeneration (Table 2, Figure S4, C and D). In contrast, the extent of CCVD attenuation within areas of matched degeneration was moderately correlated with the increasing size of the respective area; however it was not significant after correcting for multiple comparisons ($r = -0.48$) (Table 2, Figure S4A). The CCVDs within areas of no degeneration (intact IS/OS and RPE) in STGD patients (97.6 ± 0.38%) was significantly greater than that in areas of matched degeneration ($P = 0.0004$) but not significantly different than areas of isolated IS/OS or RPE degeneration (Figure 5C). Even though the CCVD within seemingly intact areas of retina and RPE in STGD was not significantly different than normal subjects (STGD: 97.6 ± 0.38 vs normal: 99.0 ± 0.17%), it had a range with a lower limit (STGD: 93.8 to 99.6% vs normal: 97.9–99.6%), and there was moderate correlation of worsening CCVD within diminishing areas of intact structure that was just beyond the threshold for significance after Bonferroni correction ($r = 0.68$) (Table 2, Figure S4B). Taken together, these data suggest that both intralesional and extralesional CCVDs tended to worsen as the degenerative lesion expanded, which may explain why the total CCVD was much more strongly correlated with the size of the degenerative lesion.

DISCUSSION

THE EN FACE OCT AND OCTA FINDINGS IN STGD HAVE BEEN reported previously, however, here we used an en face slab projection method and boundary maps to create IS/OS loss or RPE atrophy masks that not only allowed for analysis of total IS/OS loss or RPE atrophy but also IS/OS-RPE composite masks that allowed for the analysis of regions with isolated IS/OS loss, isolated RPE atrophy, matched IS/OS and RPE degeneration or intact IS/OS and RPE. These masks allowed for quantification and correlation analysis

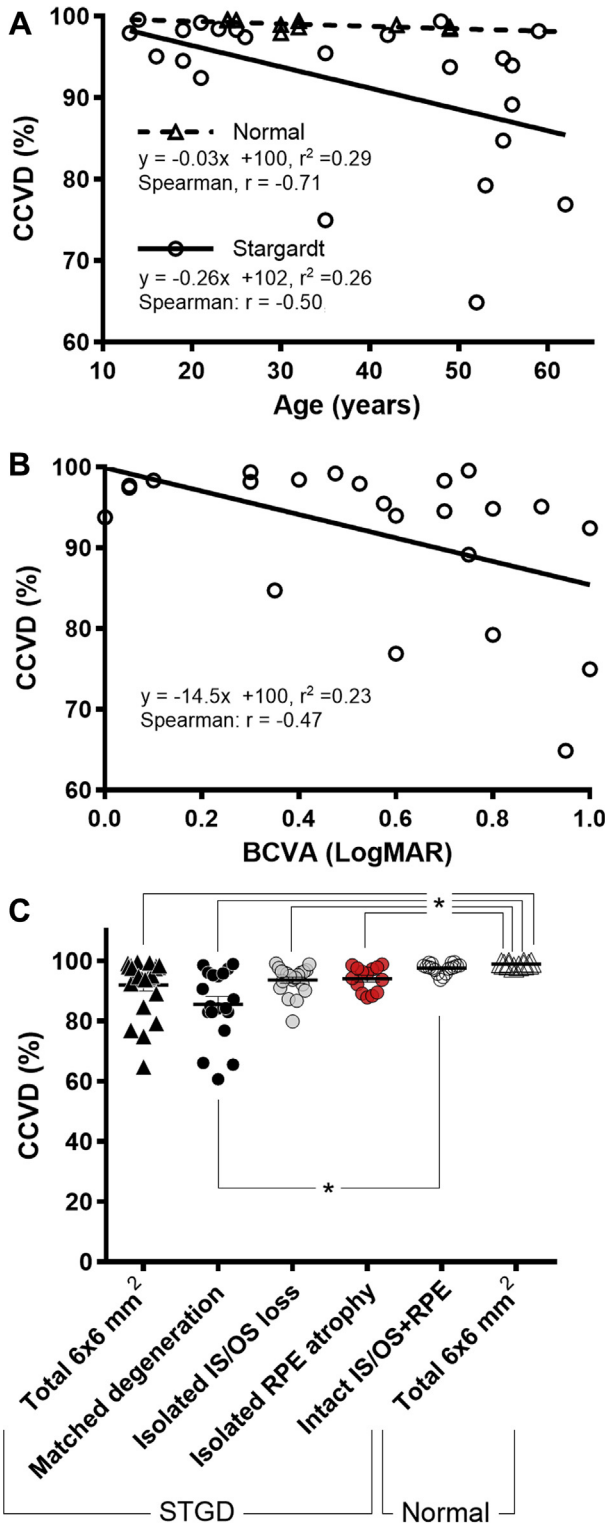

FIGURE 5. Age or BCVA versus CCVD and composite mask analysis of CCVD. (A and B) Scatter plot of age or BCVA versus CCVD shows a moderate correlation of declining CCVD with increasing age or decreasing BCVA (increasing logMAR); however, statistical significance was limited by multiple comparisons (Table 2). (C) Total CCVD from normal subjects were significantly greater than total CCVD and the CCVD within the various region types of degeneration in Stargardt patients, except for areas of intact IS/OS junction and RPE. The CCVDs within intact areas were significantly greater than the CCVD within areas of matched degeneration in Stargardt patients. The solid line with an error bar represents means and 95% confidence interval. *P ≤ 0.05. BCVA = best corrected visual acuity; CCVD = choriocapillaris vessel density; IS/OS = inner segment/outer segment.

among different region types of degeneration, as it pertains to area of degeneration, CCVD, age, and BCVA.

With regard to en face OCT, Sodi and associates,[39] Greenstein and associates,[35] and Melillo and associates[40] published various observations regarding RPE atrophy and IS/OS attenuation using various slab projection techniques. Both Sodi and associates[39] and Greenstein and associates[35] used slab methods similar to those in our study to produce en face projections of the IS/OS layer, whereas Melillo and associates[40] measured the transverse extent of IS/OS loss on OCT B-scans. All 3 groups used a sub-RPE slab projection method to create en face images of the RPE atrophy by visualizing light penetration into the choroid. The sub-RPE method favors the detection of areas of severe RPE atrophy with obvious light penetration, whereas our RPE slab method measures apical RPE signal which may be more sensitive to a wider spectrum of RPE thinning. Another group, Gomes and associates[41] performed diameter measurements of foveal IS/OS and RPE atrophy on transverse OCT B-scans. Despite the differing methods and different cohort sizes (Sodi and associates,[39] n = 32; Greenstein and associates,[35] n = 16; Melillo and associates,[40] n = 98; and Gomes and associates,[41] n = 11), all 4 groups found that the extent of IS/OS loss was greater than that of RPE atrophy, which is consistent with our findings. Furthermore, we show here, for the first time to our knowledge, a strong correlation wherein IS/OS loss is 1.6 times more widespread than RPE atrophy. Taken together with our observation that isolated RPE does not contribute significantly to overall degeneration, these structural studies support the theory that photoreceptor outer segment degeneration generally occur before RPE atrophy and not vice-versa in STGD.

Loss of CC in STGD has also been shown in prior OCTA studies.[42–47] Battaglia Parodi and associates[46] showed that CCVD was worse in STGD eyes that had chorioretinal atrophy,[46] and both Pellegrini and associates[42] and Muller and associates[47] found that the CC flow signal was visibly diminished within areas of RPE atrophy in STGD but not outside the areas of RPE atrophy.[42,47] Similar to these prior studies, the CCVD within areas of isolated RPE atrophy in our STGD patients was significantly lower than normal, but we also showed the same thing in areas of isolated IS/OS loss. Moreover, we found that the CCVD in areas of combined RPE and IS/OS attenuation tended to be even more abnormal,

supporting the theory that the degeneration of both layers is synergistically associated with CC attenuation in STGD. Furthermore, our data showed that the extent of total CCVD attenuation was strongly correlated with the magnitude of RPE degeneration, as well as with photoreceptor degeneration.

In addition, de Carlo and associates[43] reported that areas of abnormal CC appeared to be smaller than the corresponding regions of RPE and photoreceptor loss in STGD. In our experience, the boundary between abnormal and normal CCVD areas was difficult to visualize and map reliably, so our study did not quantify the size of the CCVD defect. However, using composite IS/OS-RPE boundary masks, we demonstrated that the total CCVD was much more strongly correlated than intralesional CCVD to the size of the degenerative lesion, which suggests that extralesional CCVD may contribute to the level of total CCVD attenuation in STGD. Our results contradict the findings of de Carlo and colleagues[43] but are indirectly supported by the microperimetry studies of Strauss and associates[48] showing extralesional areas of decreased cone and rod-dependent sensitivity. Taken together with the findings of Strauss and colleagues,[48] our results suggest that relative photoreceptor dysfunction with mild CC attenuation may precede lesion expansion in STGD.

Prior studies have reported correlations of IS/OS loss, RPE atrophy, or CCVD with age and/or BCVA.[40,44,45,49] Arepalli and associates[49] reported that foveal IS/OS atrophy was inversely correlated with visual acuity, and Melillo and associates[40] have shown that macular RPE atrophy area increases exponentially with age in STGD. Ratra and associates[44] and Mastropasqua and associates[45] showed that choriocapillaris vascular index and CCVD were correlated with decreasing visual acuity and parafoveal macular thickness, respectively.[44,45] Similarly, our data showed a trend towards a moderate correlation between IS/OS loss, RPE atrophy, and CCVD attenuation with age or BCVA, however our statistical significance was limited by multiple comparisons. It is also likely that our cohort was more heterogeneous than other studies due to inherent differences in sampling error, wherein the composition of patients with late onset disease and foveal sparing versus those with early onset disease with foveal atrophy would directly influence these correlations. Stratification of our data set according to these patient types was limited by access to historical records and inaccurate recall in our older patients. Our cohort (n = 23) was also smaller than that of Melillo (n = 98) and Ratra (n = 39), but greater than Arepalli and associates[49] (n = 17) and Mastropasqua and associates[45] (n = 12).

This study was limited by a relatively small sample size, but STGD is a rare disease, and future multicenter studies would be required to obtain larger datasets. Although 7 subjects were excluded from composite masks and correlation analyses due to floor effect, the data from the remaining 16 patients were still sufficient to show statistically significant correlations even with Bonferroni correction that resulted in a much stricter P value of ≤ 0.0013 for determination of significance (Table 2). In addition, determining the slab position and grading of primary masks were manual processes and time-consuming; however, we implemented a standardized protocol, and the degree of inter-grader agreement was extremely high. Future work will be directed toward developing algorithms to automate these processes and determine its agreement with manual analysis, as well as increasing the number of patients. This study is also limited by its cross-sectional nature, and future longitudinal studies will be helpful in confirming the findings of our study. The conclusions of this study were drawn solely on findings from retinal structure alone, so future structure-function studies will also be necessary to assess the dynamics of photoreceptor and RPE dysfunction with degeneration in STGD.

We show quantitative evidence that photoreceptor and RPE degeneration exhibit a strong relationship wherein photoreceptor IS/OS loss is 1.6-fold more widespread than RPE atrophy, supporting the theory that photoreceptor degeneration may precede RPE in STGD. Furthermore, our study also showed that IS/OS loss and RPE atrophy contribute synergistically to CCVD attenuation, but extralesional CCVD also tended to be abnormal, which may be associated with possible early dysfunction of photoreceptor or RPE. These findings, along with the techniques used in this study, may be of considerable utility in determining novel endpoints for gene and stem cell therapy clinical trials.

FUNDING/SUPPORT: SUPPORTED BY AN UNRESTRICTED GRANT FROM RESEARCH TO PREVENT BLINDNESS, NEW YORK, NEW York, USA; a Career Development Award and a William and Mary Greve Special Scholar Award (to Y.J.); a Foundation Fighting Blindness, Columbia, Maryland, USA, center grant/C-Cl-0711-0534-OHSU01; Enhanced Career Development Award/CD-NMT-0914-0659-OHSU (to M.E.P.); Career Development Award/CD-NMT-0714-0648 (to P.Y.); National Institutes of Health, Bethesda, MD, USA, Core Grants P30 Ey010572 (to C.E.I.), R01 EY027833 (to Y.J.), R01 EY024544 (to Y.J.), DP3 DK104397 (to Y.J.), K08 EY026650 (to P.Y.), and 5R24EY022023 (subaward); and Choroideremia Research Foundation, Springfield, Massachusetts (to M.E.P.).

Financial Disclosures: Yali Jia and David Huang have financial interests in Optovue. David Huang receives research funding, material support, speaker honoraria, and travel support from Optovue. Richard Weleber and Mark Pennesi have commercial relationships and are members of the scientific advisory boards for the Foundation Fighting Blindness. Simon Gao is an employee of Genentech. Miao Zhang is an employee of Topcon. Paul Yang is a consultant for Astellas.

The following authors have no financial disclosures: Talal Alabduljalil, Rachel C. Patel, Abdullah A. Alqahtani, Simon S. Gao, Michael J. Gale, Miao Zhang, Pei-Wen Chiang, Rui Chen, Jun Wang, and Paul Yang. All authors attest that they meet the current ICMJE criteria for authorship.

REFERENCES

1. Savary S, Allikmets R, Denizot F, et al. Isolation and chromosomal mapping of a novel ATP-binding cassette transporter conserved in mouse and human. *Genomics* 1997;41:275–278.
2. Stargardt K. Über familiäre, progressive Degeneration in der Maculagegend des Auges. *Albrecht von Graefes Archiv für Ophthalmologie* 1906;71:534–550.
3. Cremers FP, van de Pol DJ, van Driel M, et al. Autosomal recessive retinitis pigmentosa and cone-rod dystrophy caused by splice site mutations in the Stargardt's disease gene ABCR. *Hum Mol Genet* 1998;7:355–362.
4. Maugeri A, Klevering BJ, Rohrschneider K, et al. Mutations in the ABCA4 (ABCR) gene are the major cause of autosomal recessive cone-rod dystrophy. *Am J Hum Genet* 2000;67:960–966.
5. Rotenstreich Y, Fishman GA, Anderson RJ. Visual acuity loss and clinical observations in a large series of patients with Stargardt disease. *Ophthalmol* 2003;110:1151–1158.
6. Franceschetti A, Francois J. [Fundus flavimaculatus]. *Arch Ophtalmol Rev Gen Ophtalmol* 1965;25:505–530.
7. Westeneng-van Haaften SC, Boon CJ, Cremers FP, Hoefsloot LH, den Hollander AI, Hoyng CB. Clinical and genetic characteristics of late-onset Stargardt's disease. *Ophthalmol* 2012;119:1199–1210.
8. Lambertus S, van Huet RA, Bax NM, et al. Early-onset Stargardt disease: phenotypic and genotypic characteristics. *Ophthalmol* 2015;122:335–344.
9. Armstrong JD, Meyer D, Xu S, Elfervig JL. Long-term follow-up of Stargardt's disease and fundus flavimaculatus. *Ophthalmol* 1998;105:448–457. discussion 457–448.
10. Noble KG, Carr RE. Stargardt's disease and fundus flavimaculatus. *Arch Ophthalmol* 1979;97:1281–1285.
11. Yatsenko AN, Shroyer NF, Lewis RA, Lupski JR. Late-onset Stargardt disease is associated with missense mutations that map outside known functional regions of ABCR (ABCA4). *Hum Genet* 2001;108:346–355.
12. Fujinami K, Lois N, Davidson AE, et al. A longitudinal study of stargardt disease: clinical and electrophysiologic assessment, progression, and genotype correlations. *Am J Ophthalmol* 2013;155:1075–1088.e13.
13. Lois N, Holder GE, Bunce C, Fitzke FW, Bird AC. Phenotypic subtypes of Stargardt macular dystrophy-fundus flavimaculatus. *Arch Ophthalmol* 2001;119:359–369.
14. Martinez-Mir A, Paloma E, Allikmets R, et al. Retinitis pigmentosa caused by a homozygous mutation in the Stargardt disease gene ABCR. *Nat Genet* 1998;18:11–12.
15. Bayes M, Goldaracena B, Martinez-Mir A, et al. A new autosomal recessive retinitis pigmentosa locus maps on chromosome 2q31-q33. *J Med Genet* 1998;35:141–145.
16. Molday RS. Insights into the molecular properties of abca4 and its role in the visual cycle and Stargardt disease. *Prog Mol Biol Transl Sci* 2015;134:415–431.
17. Quazi F, Molday RS. Differential phospholipid substrates and directional transport by ATP–binding cassette proteins ABCA1, ABCA7, and ABCA4 and disease-causing mutants. *J Biol Chem* 2013;288:34414–34426.
18. Quazi F, Lenevich S, Molday RS. ABCA4 is an N-retinylidene-phosphatidylethanolamine and phosphatidylethanolamine importer. *Nat Commun* 2012;3:925.
19. Sun H, Smallwood PM, Nathans J. Biochemical defects in ABCR protein variants associated with human retinopathies. *Nat Genet* 2000;26:242–246.
20. Zhong M, Molday LL, Molday RS. Role of the C terminus of the photoreceptor ABCA4 transporter in protein folding, function, and retinal degenerative diseases. *J Biol Chem* 2009;284:3640–3649.
21. Sparrow JR, Zhou J, Ben-Shabat S, Vollmer H, Itagaki Y, Nakanishi K. Involvement of oxidative mechanisms in blue-light-induced damage to A2E-laden RPE. *Invest Ophthalmol Vis Sci* 2002;43:1222–1227.
22. Mata NL, Weng J, Travis GH. Biosynthesis of a major lipofuscin fluorophore in mice and humans with ABCR-mediated retinal and macular degeneration. *Proc Natl Acad Sci U S A* 2000;97:7154–7159.
23. Sparrow JR, Boulton M. RPE lipofuscin and its role in retinal pathobiology. *Exp Eye Res* 2005;80:595–606.
24. Radu RA, Mata NL, Bagla A, Travis GH. Light exposure stimulates formation of A2E oxiranes in a mouse model of Stargardt's macular degeneration. *Proc Natl Acad Sci U S A* 2004;101:5928–5933.
25. Sparrow JR, Nakanishi K, Parish CA. The lipofuscin fluorophore A2E mediates blue light-induced damage to retinal pigmented epithelial cells. *Invest Ophthalmol Vis Sci* 2000;41:1981–1989.
26. Lenis TL, Sarfare S, Jiang Z, Lloyd MB, Bok D, Radu RA. Complement modulation in the retinal pigment epithelium rescues photoreceptor degeneration in a mouse model of Stargardt disease. *Proc Natl Acad Sci U S A* 2017;114:3987–3992.
27. Radu RA, Hu J, Jiang Z, Bok D. Bisretinoid-mediated complement activation on retinal pigment epithelial cells is dependent on complement factor H haplotype. *J Biol Chem* 2014;289:9113–9120.
28. Radu RA, Hu J, Yuan Q, et al. Complement system dysregulation and inflammation in the retinal pigment epithelium of a mouse model for Stargardt macular degeneration. *J Biol Chem* 2011;286:18593–18601.
29. Smit-McBride Z, Oltjen SL, Radu RA, et al. Localization of complement factor H gene expression and protein distribution in the mouse outer retina. *Mol Vis* 2015;21:110–123.
30. Srinivasan VJ, Adler DC, Chen Y, et al. Ultrahigh-speed optical coherence tomography for three-dimensional and en face imaging of the retina and optic nerve head. *Invest Ophthalmol Vis Sci* 2008;49:5103–5110.
31. Wojtkowski M, Srinivasan V, Fujimoto JG, et al. Three-dimensional retinal imaging with high-speed ultrahigh-resolution optical coherence tomography. *Ophthalmol* 2005;112:1734–1746.
32. Jia Y, Bailey ST, Hwang TS, et al. Quantitative optical coherence tomography angiography of vascular abnormalities in the living human eye. *Proc Natl Acad Sci U S A* 2015;112:E2395–E2402.
33. Jain N, Jia Y, Gao SS, et al. Optical coherence tomography angiography in choroideremia: correlating choriocapillaris loss with overlying degeneration. *JAMA Ophthalmol* 2016;134:697–702.
34. Zhang M, Wang J, Pechauer AD, et al. Advanced image processing for optical coherence tomographic angiography of macular diseases. *Biomed Opt Express* 2015;6:4661–4675.

35. Greenstein VC, Nunez J, Lee W, et al. A comparison of en face optical coherence tomography and fundus autofluorescence in Stargardt disease. *Invest Ophthalmol Vis Sci* 2017;58:5227–5236.
36. Jia Y, Tan O, Tokayer J, et al. Split-spectrum amplitude-decorrelation angiography with optical coherence tomography. *Opt Express* 2012;20:4710–4725.
37. Wang J, Zhang M, Hwang TS, et al. Reflectance-based projection-resolved optical coherence tomography angiography [invited]. *Biomed Opt Express* 2017;8:1536–1548.
38. Ren Y, Jia Y, Dong N, et al. Guided-wave second harmonics in Nd:YCOB optical waveguides for integrated green lasers. *Opt Lett* 2012;37:244–246.
39. Sodi A, Mucciolo DP, Cipollini F, et al. En face OCT in Stargardt disease. *Graefes Arch Clin Exp Ophthalmol* 2016;254:1669–1679.
40. Melillo P, Testa F, Rossi S, et al. En face spectral-domain optical coherence tomography for the monitoring of lesion area progression in Stargardt disease. *Invest Ophthalmol Vis Sci* 2016;57:OCT247–OCT252.
41. Gomes NL, Greenstein VC, Carlson JN, et al. A comparison of fundus autofluorescence and retinal structure in patients with Stargardt disease. *Invest Ophthalmol Vis Sci* 2009;50:3953–3959.
42. Pellegrini M, Acquistapace A, Oldani M, et al. Dark atrophy: an optical coherence tomography angiography study. *Ophthalmol* 2016;123(9):1879–1886.
43. de Carlo TE, Adhi M, Salz DA, et al. Analysis of choroidal and retinal vasculature in inherited retinal degenerations using optical coherence tomography angiography. *Ophthalmic Surg Lasers Imaging Retina* 2016;47(2):120–127.
44. Ratra D, Tan R, Jaishankar D, et al. Choroidal structural changes and vascularity index in Stargardt disease on swept source optical coherence tomography. *Retina* 2018;38(12):2395–2400.
45. Mastropasqua R, Toto L, Borrelli E, et al. Optical coherence tomography angiography findings in Stargardt Disease. *PLoS One* 2017;12:e0170343.
46. Battaglia Parodi M, Cicinelli MV, Rabiolo A, Pierro L, Bolognesi G, Bandello F. Vascular abnormalities in patients with Stargardt disease assessed with optical coherence tomography angiography. *Br J Ophthalmol* 2017;101(6):780–785.
47. Muller PL, Pfau M, Moller PT, et al. Choroidal flow signal in late-onset Stargardt disease and age-related macular degeneration: an OCT-angiography study. *Invest Ophthalmol Vis Sci* 2018;59(4):AMD122–AMD131.
48. Strauss RW, Kong X, Bittencourt MG, et al. Scotopic microperimetric assessment of rod function in Stargardt disease (SMART) study: design and baseline characteristics (report no. 1). *Ophthalmic Res* 2019;61(1):36–43.
49. Arepalli S, Traboulsi EI, Ehlers JP. Ellipsoid zone mapping and outer retinal assessment in Stargardt disease. *Retina* 2018;38:1427–1431.